Ion Migration and Role of Pre-conditioning cycles in the Stabilization of the J-V Characteristic of Inverted Hybrid Perovskite Solar Cells

Michele De Bastiani, Giorgio Dell'Erba, Marina Gandini, Valerio D'Innocenzo, Stefanie Neutzner, Ajay Ram Srimath Kandada, Giulia Grancini, Maddalena Binda, Mirko Prato, James M. Ball, Mario Caironi and Annamaria Petrozza**

M. De Bastiani, G. Dell'Erba, V. D'Innocenzo, M. Gandini, Dr G. Grancini, Dr. J. M. Ball, Dr. M. Binda, Dr. M. Caironi, Dr. A. Petrozza
Center for Nano Science and Technology @PoliMi, Istituto Italiano di Tecnologia, Milan 20133, Italy
E-mail: annamaria.petrozza@iit.it, mario.caironi@iit.it

M. De Bastiani
Università degli Studi di Padova, Padova 35131, Italy

G. Dell'Erba
Dipartimento di Elettronica, Informazione e Bioingegneria, Politecnico di Milano, Milan 20133, Italy

M. Gandini, V. D'Innocenzo, Stefanie Neutzner
Dipartimento di Fisica, Politecnico di Milano, Milan 20133, Italy

Dr Mirko Prato
Department of Nanochemistry, Istituto Italiano di Tecnologia, via Morego, 30, 16163 Genova, Italy

Keywords: perovskite solar cells, hysteresis, PCBM, charge extracting layers

Solution-processable hybrid perovskite semiconductors have risen to the forefront of photovoltaics research, offering the potential to combine low-cost fabrication with high power-conversion efficiency. Originally used in dye-sensitized solar cell technology, the first architectures saw the use of TiO_2, both in the form of mesoporous and compact films, as an electron extracting layer.[1] Further development has been driven by empirical optimization strategies and testing of a variety of different architectures.[2, 3, 4, 5] One of these promising

architectures uses fully organic buffer layers, which, first of all, brings the advantage of low temperature processing.[6] The intention of understanding whether some architectures of perovskite-based devices may outperform others in terms of power conversion efficiency has been the initial driving force for most research groups. However, the observation of slow transient and hysteretic effects observed in perovskite-absorber devices, which severely affects current density–voltage (*J-V*) measurements and efficiency determination, has further stimulated deeper exploration of the working mechanisms of the devices.[7, 8, 9] Several groups have recently and independently demonstrated that, by applying an electric field across a pristine film of 3D hybrid perovskites of different chemical composition, a self-sustained field is induced in the semiconductor as a consequence of ion migration towards the electrode regions.[10, 11, 12, 13] The formation of a self-sustained internal field upon device polarization is also in good agreement with the observations reported by Z-K Tan *et al.* when testing perovskite-based light emitting diodes.[14] This concept has also been the base of the explanation proposed by W. Tress *et al.* for the rate-dependent hysteresis seen in current-voltage scans of solar cells.[15] So far reports suggest that transient electrical characteristics are due to a polarization response of the perovskite active layer that results in changes in the photocurrent extraction efficiency of the device.[11 , 15] However, it must be noted that a variety of dynamics have been reported, which differ in magnitude and time scale, depending both on the specific device architecture and, in particular, on the adopted charge extraction layer.[7, 9] This indicates that contact interfaces have a considerable effect on transients in perovskite based devices.

In this communication we investigate the role played by charge extracting layers on the slow transient behavior of $CH_3NH_3PbI_3$ perovskite based solar cells. Such transients, which typically affect both short circuit currents and open circuit voltage of hysteretic devices, are found to notably modify the open circuit voltage also in the very first *J-V* scans of so called "hysteresis-free" devices integrating a Phenyl-C61-butyric acid methyl ester (PCBM) charge

extraction layer. Here a pre-conditioning of the device, i.e. a repetition of *J-V* scans, is needed to achieve completely stable *J-V* characteristics under illumination. In particular, we find that under device operation, iodide ions migrate to the electron extracting layer. While ions transport is typically associated with charge extraction efficiency, we first show that the use of an organic extraction layer such as PCBM, albeit not hampering ions motion, evidently improves charge extraction with respect to interfaces involving compact TiO_2, in agreement with what is suggested in other seminal investigations,[16,24] and makes the short circuit current density virtually insensitive to the transient phenomena related to ions migration. Moreover, while self doping of the perovskite film close to the contact has been generally put forward in the study of transient phenomena, [12, 13] here we show that ions can specifically interact with the organic electron extracting layer, inducing electronic doping and that such I^-/PCBM interaction is at the origin of the pre-conditioning requirement for stabilizing the device and for improving its open circuit voltage with respect to the first scan.

In **Figure 1** we report the *J-V* characteristics of three different device architectures as a function of the scanning rate and direction. Figure 1.a shows the characteristics of a nanostructured architecture where a compact layer of TiO_2 and 2,2´,7,7´-tetrakis-(N,N-di-p-methoxy phenylamine) 9,9´- spirobifluorene (spiro-OMeTAD) are employed for the extraction of the electrons and holes respectively, and a mesoporous structure of Al_2O_3 nanoparticles is employed as a scaffold for the perovskite. Figure 1.b shows a nanostructured architecture, again, where the meso-alumina is substituted with a scaffold of TiO_2 nanoparticles. Then, Figure 1.c shows the so-called inverted architecture where layers of PEDOT:PSS and PCBM for the collection of holes and electrons are adopted, respectively. The figures of merit of these devices and details about the their testing procedures are reported in **Table 1**. The architecture encompassing the mesoporous alumina layer and a flat TiO_2 as electron extracting layer is affected by severe hysteresis features, with a strong reduction of the photocurrent when the scanning rate is slowed down. The phenomenon is

attenuated by replacing the mesoporous alumina with a mesoporous TiO_2 extraction layer. This effect finally becomes negligible when electron extraction occurs at the interface with PCBM, in an inverted structure. Such a trend already highlights a role of the charge extraction interface in the response of the device to slow transient phenomena.[16, 17]

We want now to emphasize that the curves of Figure 1 have been obtained after a specific conditioning. In particular, the curves of Figure 1 a and b are observed only by scanning the device starting from a pre-biasing, *i.e.* a bias voltage applied prior to *J-V* scans, under light conditions at 1.4 V for 10 s, without which photocurrent is highly suppressed. On the other hand, even the hysteresis-free behaviour of the inverted device of Figure 1 c is obtained only after scanning the *J-V* characteristic of the same device several times, as shown in **Figure 2**, while a pre-bias at 1.4 V under light is highly detrimental. Though it has been recently proposed that PCBM deposited on top of the perovskite reduces the density of trap states, which are indicated as the origin of hysteresis, [16,18] during the first *J-V* scans performed on a freshly made device, the latter exhibits clear hysteresis when scanning the voltage from forward-bias to short-circuit and back. By repeating the measurement this difference is reduced, ultimately becoming negligible and producing the hysteresis free scans reported in Fig. 1c. In particular, while the short circuit current is almost unaffected upon several scans, the open-circuit voltage needs a few cycles to be stabilized: evidently, what is at the base of the transient phenomena does not necessarily affects both parameters at the same time. A similar phenomenon is also present in the dark *J-V* curves (see Figure S1 of the SI). This shows the clear need of some *pre-conditioning J-V cycles* to reach a stable performance, even in presence of PCBM.

With the intent of clarifying the role of PCBM in such peculiar behaviour, first, we investigate the reason behind the short circuit current stability compared to the cells integrating a TiO_2 layer. **Figure 3.a** compares the photoluminescence (PL) quenching of $CH_3NH_3PbI_3$ forming a flat junction with TiO_2 and PCBM. Comparing these dynamics with the PL decay of a

$CH_3NH_3PbI_3$ polycrystalline film deposited on a glass substrate, one can immediately notice that the PCBM induces a considerable quenching, while in presence of TiO_2 quenching is nearly negligible (please note that crystal size effects cannot explain such large change in PL dynamics[23]). As we can safely assume that that the perovskite surface will be improved upon PCBM deposition[18] rather than inducing interface trap states, we can conclude that PCBM provides superior charge extraction properties with respect to TiO_2. To better contextualize these results with what is generally observed in working devices, in Figure 3.b we show the PL dynamics of CH_3NH_3PbI embodied in a full device architecture (i.e. PEDOT:PSS/ $CH_3NH_3PbI_3$ /PCBM) at short circuit condition. In particular we compare the PL decay, at early times after photo-excitation (ps-ns), before and after a pre-biasing the device at 1V. The dynamics do not change dramatically. Therefore we conclude that electron transfer is not affected by polarizing the perovskite film, consistently with the observed short-circuit current stability.

For comparison, in Figure S3 we also report the photo-bleaching (PB) dynamics, in the ps-ns time window, of the same hybrid perovskite, probed in devices where spiro-OMeTAD was used as hole extracting material, while PCBM or TiO_2 are used as electron extracting layers[24] and we compare them with the PL dynamics taken from the PEDOT:PSS/ $CH_3NH_3PbI_3$ /PCBM device. The photo-bleach originates from the transparency induced at the onset of the optical absorption of a semiconductor upon photo-excitation after population of the bottom of conduction band and top of the valence band respectively, thus it will follow the electron and holes population dynamics in the semiconductor[25,26]. When the PCBM is used, the PB dynamics well follow the PL dynamics of the PEDOT:PSS/Perovskite/PCBM devices and they are not affected by pre-biasing of the device. On the other hand, in presence of TiO_2, the charge extraction becomes faster, and comparable to those in presence of PCBM, only upon pre-biasing. This is indicating, first of all, that the electron extracting interface is the most sensitive and critical one in state-of-the art perovskite solar cell architectures as electron

extraction strongly depends on the nature of the interface and on the thin film polarization condition, while no significant change is observed by changing the hole extracting layer. Then, importantly, we have also the evidence that, differently from flat TiO_2, PCBM provides such good electronic contacts at the interface with perovskites that the extraction is not influenced by pre-biasing of the device. This well explains the steady state photocurrent stability found in presence of PCBM.

Then, we move our investigation to the role of pre-conditioning on solar cell open-circuit voltage. To gain insight in the stabilization process highlighted in Fig.2, we have performed a systematic investigation on the poling (i.e. polarization of the semiconductor) effects on pristine perovskite (**Figure 4.a**) and on a perovskite/PCBM bi-layer (**Figure 4.b**) deposited on planar symmetric gold contacts, defining a 20 μm long channel (see sketch in Figure S2 of SI). We performed the poling of both samples by biasing them in dark conditions to be able to disentangle the effects strictly related to the device polarization from eventual light induced effects. All the experiments were performed in inert atmosphere. Without any pre-biasing, the current-voltage (*I-V*) characteristics recorded from 0 V to + 28 V and from 0 V to – 28 V on pristine perovskite and bi-layer samples are symmetric, with similar current values (Figure 4.a and 4.b, black lines). When the two samples are pre-biased by applying a field of 1.4 $V\mu m^{-1}$, the symmetry in the curves is lost and the current exhibits a rectifying behaviour. This effect is a consequence of the partial positive and negative charges induced at the contacts that hamper the injection of charge at an applied voltage which is opposite with respect to the pre-biasing, as suggested by Huang *et al.*.[10] Furthermore it must be noted that by inverting the polarization between the two electrodes (indicated henceforth as positive and negative poling), the switching of the *I-V* characteristic is not instantaneous, as it requires minutes-to-hours in order to recover the initial condition. Huang *et al.* reported this effect for the first time for pristine perovskite under light illumination.[10] They concluded that it is the result of ions drifting through the perovskite, forming two doped regions, *n* and *p*, next to the

electrodes, according to the voltage applied. Interestingly, Figure 4.b shows that the presence of PCBM deposited on top of the perovskite layer does not apparently hamper the ions drift, as the loss of symmetry in the curves demonstrates. The only difference induced by the presence of PCBM is an increased value of the forward current under poling conditions. From these results we can summarize that: *i*) the ion migration, proposed to be responsible for the formation of an internal field within the planar device with symmetric contacts, is observable not only under light illumination (see Figure S4 in SI) but also in the dark, thus excluding a role of photoexcitation; *ii*) under polarization, the presence of PCBM does not prevent the ions drifting. Thus, ions diffusion/drifting is still present in solar cells with a PCBM electron extracting layer, even if the short circuit current (*i.e.* charge extraction) is stable upon scanning.

The presence of PCBM in the planar sample increases the absolute values of the forward current. Though one can assume that PCBM diffusion in the perovskite thin film may induce a better morphology (compactness) of the thin film,[18] we can exclude it as the origin of the enhanced current because, without pre-biasing, the current values are similar with or without PCBM.

To pin down the origin of the enhanced forward current when the perovskite/PCBM bilayer is pre-biased, in Figure 4c we investigate the time evolution of the current upon polarization, with and without PCBM, on a time scale of hundreds of seconds for both samples (please note that these are twin fresh sample of the ones studied in Figures 4.a and 4.b). Under poling, the pristine film (full dots, black line) shows an enhancement in current in the first 60 seconds until a plateau value is reached. We attribute the initial rising to the creation of the doped junction, via ions drifting, which is completed when the current stabilizes. In the presence of PCBM (full dots, red line) the transient dynamic is slowed down; however, the absolute value of the current increases without reaching a stabilized point in our time scale. This behaviour is not symmetric when the poling is instantaneously inverted between the two electrodes

(hollow circles). In this condition the absolute values of the currents are strongly reduced and slowly increase for both films, again with a slower dynamic for the perovskite/PCBM film. Such slow dynamics clarify that the current enhancement in the presence of PCBM is also related to the migration of ions. Upon fabrication of the perovskite/PCBM bilayer we can assume that the small organic molecules intercalate the perovskite grain of the polycrystalline film, thus forming also lateral PCBM/perovskite interfaces. These observations lead us to hypothesize that upon polarization, ions do interact with the organic compound, increasing the overall conductivity of the film. In the solar cell with PCBM as electron extracting layer, since ions, along with the photogenerated carriers, drift towards the electrodes due to the built-in voltage, an interaction of such species with the extracting layers is possible. Recent experimental[28,31] and theoretical[32,33] investigations have indicated iodide ions, I-, and methyilammonium ions, MA+, as the most probable anionic and cationic species which can diffuse and/or drift within the perovskite absorber here studied.

As a consequence of the built-in field deriving by the different contacts work-function, during cell operation iodide ions, I^-, are expected to accumulate close to PCBM, while MA^+ close to the hole extracting contact.[19] The actual possibility for MA^+ to drift under the influence of a field is currently being debated. Recent theoretical studies predict a high activation barrier (0.84 eV)[32], while others derive a barrier consistent with MA^+ motion (0.46 eV)[33]. Some experimental work, such as the one by Huang *et al*.[28] agree with the latter, probing an accumulation of MA^+ upon polarization of $MAPbI_3$ thin film (in air) at the negatively polarized electrode. However they do not exclude the presence of I- rich areas due to a poor sensitivity of their experimental technique to such species. There is instead theoretical agreement on the migration of I^-,[32, 33] with however limited experimental evidence. In the following we first address the eventual drifting of iodide as an effect of a field developing across the semiconductor, and we then investigate its interaction with PCBM. To prove the nature of the negatively charged mobile ions migrating within the $MAPbI_3$, we biased, in dark

and nitrogen atmosphere, a sample composed of a pair of planar and symmetric silver electrodes, on top of which a pristine perovskite layer was deposited . Silver has been chosen due to its selective interaction with iodide, forming metal halides compounds. **Figure 5** shows the SEM images of the thin film deposited on the metal contacts in pristine conditions (top panel) and upon biasing (bottom panel). After biasing, differently from what observed previously with the samples based on gold electrodes, we are not able to register any *I-V* curve and we observe that the area corresponding to the positively biased electrodes results damaged, while the negatively biased electrodes appear unmodified. This provides evidence of the electro-migration of the I^- ions towards the positively biased electrode and their reaction with Ag.

We move now to the investigation of the interaction of the migrating anions with PCBM. It is well reported in the literature that PCBM can interact with alkyl ammonium salts resulting in a doping of the material itself.[20] In particular these salts act as n-dopants of the fullerene derivatives, increasing their conductivity by several orders of magnitude.

We verified this effect first by measuring the conductivity of a pristine PCBM film and a PCBM film containing a controlled amount of I^-. The latter was realized by adding a methylammonium iodide (MAI) solution (10 mg/ml in isopropanol) to the pristine PCBM solution (30 mg/ml in CB) with a ratio of 1:30. In **Figure 6.a** we compare the *J-V* plot of the two films. For this test we chose symmetric gold contacts with a channel length of 200 µm in order to avoid contact resistance effects. The addition of the MAI salt to the PCBM results in a markedly increased conductivity, which changes from $6.43 \cdot 10^{-7}$ S/m for the pristine film to $4.35 \cdot 10^{-6}$ S/m for the PCBM/MAI film. This effect may be ascribed either to a chemical doping of the PCBM, *i.e.* an excess of free carriers, or to an improved mobility, or both. In order to get deeper insights we tested the electronic properties of a PCBM film and a PCBM/MAI film in top gate/bottom contact field-effect transistors (FET). By comparing the measurements (Figure 6.b) of the pristine PCBM and the MAI doped devices, we are able to

extract useful information regarding the PCBM interaction with $CH_3NH_3^+$ and I^- ions that validate the aforementioned PCBM/perovskite interaction. The extracted saturation mobility (at $V_G = V_D = 60$ V) results to be $5.9 \cdot 10^{-2}$ $cm^2V^{-1}s^{-1}$ for the pristine PCBM transistor – in agreement with literature values [19, 20]- and 0.15 $cm^2V^{-1}s^{-1}$ for the doped PCBM/ MAI device. The latter value is more than two times higher than the pristine PCBM one. The pristine PCBM device shows poorer subthreshold slope values and a higher threshold voltage (36.3 V, which reduces to 8.1 V upon doping), likely owing to deep trap states. The holes current tail exhibited at low gate voltages in the saturation regime by the pristine PCBM device ($V_D = 60$ V curve in Figure 4c) disappears in the MAI doped one, resulting in a suppressed hole conduction. At the same time, a marked increase of the non-gateable OFF current in saturation in the MAI doped devices denotes a conductivity increase of the semiconducting film, confirming the results reported above for the two terminal devices (in the linear regime the OFF currents are at the level of leakage and cannot be compared). The generally increased performances (**Table 2**) of the doped device, with respect to the pristine one, can be attributed according to literature[21] to an increased concentration of excess carriers, as a consequence of chemical doping which shifts the Fermi level closer to the LUMO level of PCBM. To confirm this we used Ultraviolet Photoelectron Spectroscopy (UPS) to investigate the energy levels of the same films used in the transistors (Figure 6.c). The limited penetration depth characteristic of UPS makes this investigation more suitable to explain the FET data, where a nanometer thick channel accumulates at the semiconductor-dielectric interface, rather than the two terminal samples data. By linear extrapolation from the high binding energy region of the spectrum we derive the position of the Fermi level for pristine PCBM and for the PCBM:MAI film to be respectively at -4.27 eV and -4.13 eV. This is a relatively small but consistent shift of the Fermi level towards the vacuum level when the methylammonium salt is added to the film, indicating a clear n-doping effect. From the Fermi level position, as a first approximation, we have estimated the charge carrier density at thermal equilibrium in both

films on the basis of a single-crystal lattice model[29]. In the case of the pristine PCBM we determined an electron density of $2.5 \cdot 10^{11}$ cm^{-3}; while for the PCBM:MAI film a concentration of $5.7 \cdot 10^{13}$ cm^{-3}, two orders of magnitude higher respect to the pristine sample (see SI for the calculations).

Thus, in the transistor deep trap states are filled by chemically introduced excess carriers, and as a consequence, for the same applied gate voltage, electrostatically accumulated carriers in the channel occupy more mobile states, thus producing a net shift in the threshold voltage and an increased field-effect mobility. These results confirm the interaction between ions and the PCBM that occurs at the interface between the perovskite and the PCBM, with the increased conductivity of the PCBM phase owing to an increased number of free carriers induced by I^- doping.

We conclude that, while the main cause of hysteretic behaviour in perovskite solar cells can be found in the formation of an internal field upon ion migration, the role of the charge extracting layer is of paramount importance in determining the device response to such transient phenomenon. Efficient charge extraction is critical to make the devices less sensitive to their *J-V* scanning history. This is especially true when monitoring the short circuit photo-current density: we have shown that by introducing a PCBM electron extracting layer, though a formation of a p-i-n junction within the perovskite layer is still expected upon cell operation, the electron transfer rate at the perovskite-PCBM layer results almost unaffected, stabilizing the short circuit current from the very first *J-V* scan. On the other hand, we provide evidence for a further phenomenon, not considered so far, which needs to be taken into account both when designing efficient perovskite solar cells and when attempting their modelling. We show that, upon ion migration, a modification of the electronic properties of PCBM occurs at the interface with the perovskite. In particular, as an effect of the built-in field, iodide migrates towards the PCBM layer and it chemically dopes the organic semiconductor, increasing its conductivity. Upon *pre-conditioning J-V* cycles, such doping contributes to

improve and stabilize the open-circuit voltage, as previously observed also for other photovoltaic technologies,[30] thus producing an overall stabilization of the device. The latter is a direct consequence of the electron transfer process between the ionic species and the organic molecule, establishing an "electrostatic trap" and reducing iodide back diffusion/drift.

We therefore believe that our work provide relevant indications for the complete rationalization of "hysteresis" by showing that parameters such as the short-circuit current and open circuit voltage are not necessarily affected by the same transient behaviours.

Since hybrid perovskites are ionic solids where ions migration is allowed by either vacancies or interstitials, charge extracting layers and their interaction with such ionic species have therefore to be carefully considered when designing highly efficient and stable devices.

Furthermore this study wants to highlight that pre-conditioning cycles are typically required to observe stable *J-V* curves. Therefore care should be taken when reporting "hysteresis free" perovskite solar cells, which is not a fully appropriate description of such pre-formed devices.

Experimental Section

Fabrication and test of Perovskite Solar Cells: MAI has been synthesized according to an established procedure [2, 4] and dissolved with $PbCl_2$ (99.999%, Sigma Aldrich) in DMF with a ratio of 3:1. Except for metallic electrodes, which have been thermally evaporated, all other layers have been deposited by spin coating. The TiO_2 compact layer is deposited, according to literature [22], directly on top of FTO-covered glasses after a previous cleaning cycle with distilled water, acetone, isopropanol (IPA) and oxygen plasma. The final thickness of the TiO_2 compact layer is 80 nm. The mesoporous scaffold of Al_2O_3 (Sigma Aldrich) and TiO_2 (Dyesol) nanoparticles are deposited directly on top of the TiO_2 compact layer with a final thickness of 300 nm. PEDOT:PSS (Clevios 4083) is deposited on clean ITO substrates with a

final thickness in of 50 nm. The mixed-halide perovskite ($CH_3NH_3PbI_{3-x}Cl_x$) is deposited at 2000 rpm for 1 min and annealed at 90 °C for 90 min for the flat substrates and annealed at 100 °C for 60 min for mesoporous scaffolds. The hole extracting layer spiro-OMeTAD is processed according to literature [2] with the addition of tert-butyl pyridine and bis-(trifluoromethane) sulfonimide lithium salt (Li-TFSI, Sigma Aldrich). PCBM (NanoC) is dissolved in anhydrous chlorobenzene - CB (30 mg/ml) and for the inverted devices it is covered by a layer of Al-doped ZnO nanoparticles in isopropanol (Nanograde). Gold and aluminium are evaporated in vacuum at $1x10^{-6}$ mbar. The J/V curves of the solar cells are recorded with a computer-controlled Keithley 2400 in air under a simulated AM1.5 spectrum provided by a class AAA Newport solar simulator. The intensity of the light is calibrated with a reference diode NREL certified with a spectral mismatch factor 0.99.

Fabrication and test of Lateral Devices: Gold and silver planar electrodes used for poling the perovskite and perovskite/PCBM bi-layers are realized on pre-cleaned glass substrate by standard lithography lift-off process. The thickness of the electrodes is 50 nm, the length of the channel is 20 μm. The mixed-halide perovskite ($CH_3NH_3PbI_{3-x}Cl_x$) is deposited directly on top of the electrodes at 2000 rpm for 1 min and annealed at 90 °C for 90 min. The gold planar electrodes used for measuring the conductivity of PCBM and PCBM:MAI blend were thermally evaporated. The length of the channel between the electrodes is 200 μm. The solutions of the pristine PCBM (30 mg/ml in CB) and PCBM:MAI 30:1 blend were spin-coated in nitrogen atmosphere. Electrical characterization of lateral devices and transistors were performed in a nitrogen glove box with an Agilent B1500 Semiconductor Parameter Analyzer.

Fabrication of Transistor 35 nm thick Au source and drain contacts, on top of a 1.7 nm thick Cr adhesion layer, were patterned on a thoroughly cleaned low alkali 1737F Corning glass substrate through a standard lithographic lift-off process. Contacts for single transistors had a channel width to length ratio (W/ L) of 10000 μm/ 20 μm. Before the semiconductor

deposition, substrates were rinsed with acetone and isopropyl alcohol. PCBM and the PCBM:MAI 30:1 solutions were both deposited in a nitrogen atmosphere from a 30 mg/ml (CB and CB/IPA) solution by spin-coating at 1000 rpm for 60 s to obtain a ~40 nm thick film. The semiconductor film was then annealed at 90 °C for 20 min to guarantee solvent drying. Cytop CTL-809M 9 % w/v solution (AGC Chemicals Europe) was adopted as the dielectric layer. A thickness of 600 nm was optimized by spinning at 4000 rpm for 90 s. After the deposition of the dielectric, samples were annealed at 80 °C for 90 min. A 80 nm thick aluminium layer was thermally evaporated through a metal shadow mask to pattern the gate electrodes.

Time-resolved Photoluminescence: the experiments were performed using a femtosecond laser source and streak camera detection system (Hamamatsu C5680) operated using a synchroscan voltage sweep module, yielding a maximum temporal resolution of ~ 3 ps. An unamplified Ti:Sapphire laser (Coherent Chameleon Ultra II) operating at 80MHz was tuned to provide pulses with central wavelengths of 700 nm, energies of ~50 nJ, temporal and spectral bandwidths of ~140fs and ~5 nm, respectively. The laser light was focused with a 75 mm focal length lens onto the sample, which was kept in vacuum atmosphere during the whole measurement. The emitted photoluminescence was collected with a doublet of lenses and focused onto the entrance slit of a spectrograph (Princeton Instrument - Acton SP2300) coupled to the streak camera. The trPL measurements were performed keeping the sample at 0V polarization, polarizing it at 1.5V and again at 0V after the polarization procedure.

Transient Absorption Spectroscopy: the output of a Coherent Micra Ti:Sapphire oscillator in conjunction with a Coherent RegA 9040 amplifier (800 nm, 40 fs pulse duration and 250 kHz repetition rate) was split into two parts. One part of the laser output pumped a Coherent collinear optical parametric amplifier to generate pump pulses at 650 nm. The other part was used as probe after white light generation in a sapphire plate. The delay between the pump and the probe pulses was controlled by a motorized delay-stage and the signal was detected

using a customized CCD-camera with electronic shutter. For the measurements, the pump beam of 1.6 nJ excitation power was focused on approximately 1 mm^2 device area. All measurements were carried out in vacuum, using a continuous flow static exchange gas cryostat (Oxford Instruments Optistat CF). For monitoring the current in short-circuit condition and applying a bias voltage, the devices were connected to a Keithley B2912A source/measure unit.

Ultraviolet Photoelectron Spectroscopy: Ultraviolet photoelectron spectroscopy (UPS) measurements were carried out with a Kratos Axis Ultra^{DLD} spectrometer using a He I (21.22 eV) discharge lamp. A -9.0 V bias was applied to the sample in order to precisely determine the low kinetic energy cut-off. The analysis were carried out with an analysis area of 55 μm in diameter, at pass energy of 10 eV and with a dwell time of 100 ms.

Supporting Information

Supporting Information is available from the Wiley Online Library or from the author.

Acknowledgements

The research leading to these results has received funding from the European Union Seventh Framework Programme [FP7/2007-2013] under grant agreement n° 604032 of the MESO project, from the EU Horizon 2020 Research and Innovation Programme under Grant Agreement N. 643238 (SYNCHRONICS) and from Fondazione Cariplo (project GREENS n. 2013-0656)".

Received: ((will be filled in by the editorial staff))
Revised: ((will be filled in by the editorial staff))
Published online: ((will be filled in by the editorial staff))

[1] a) A. Kojima, K. Teshima, Y. Shirai, T. Miyasaka, *J. Am. Chem. Soc.* **2009**, *131*, 6050.
b) H.-S. Kim, C.-R. Lee, J.-H. Im, K.-B. Lee, T. Moehl, A. Marchioro, S.-J. Moon, R. Humphry-Baker, J.-H. Yum, J. E. Moser, M. Grätzel, N.-G. Park, *Sci. Rep.* **2012**, *2*, 591.
[2] M. M. Lee, J. Teuscher, T. Miyasaka, T. N. Murakami, H. J. Snaith, *Science* **2012**, *338*, 643.
[3] a) M. Liu, M. B. Johnston, H. J. Snaith, *Nature* **2013**, *501*, 395.
b) P. Docampo, J. M. Ball, M. Darwich, G. E. Eperon, H. J. Snaith, *Nat. Commun.* **2013**, *4*, 2761.
[4] J. M. Ball, M. M. Lee, A. Hey, H. J. Snaith, *Energy Environ. Sci.* **2013**, *6*, 1739.
[5] J.-H. Im, I.-H. Jang, N. Pellet, M. Grätzel, N.-G. Park, *Nat. Nanotechnol.* **2014**, *9*, 927.
[6] a) O. Malinkiewicz, C. Roldán-Carmona, A. Soriano, E. Bandiello, L. Camacho, M. K. Nazeeruddin, H. J. Bolink, *Adv. Energy Mater.* **2014**, *4*, 1400345.
b) O. Malinkiewicz, A. Yella, Y. H. Lee, G. M. M. Espallargas, M. Graetzel, M. K. Nazeeruddin, H. J. Bolink, *Nat. Photonics* **2014**, *8*, 128.
c) D. Liu, T. L. Kelly, *Nat. Photonics* **2013**, *8*, 133.
[7] H. J. Snaith, A. Abate, J. M. Ball, G. E. Eperon, T. Leijtens, N. K. Noel, S. D. Stranks, J. T.-W. Wang, K. Wojciechowski, W. Zhang, *J. Phys. Chem. Lett.* **2014**, *5*, 1511.
[8] a) R. Gottesman, E. Haltzi, L. Gouda, S. Tirosh, Y. Bouhadana, A. Zaban, E. Mosconi, F. De Angelis, *J. Phys. Chem. Lett.* **2014**, *5*, 2662.
b) H. S. Kim, N.-G. Park, *J. Phys. Chem. Lett.* **2014**, *5*, 2927.
[9] E. L. Unger, E. T. Hoke, C. D. Bailie, W. H. Nguyen, A. R. Bowring, T. Heumuller, M. G. Christoforo, M. D. McGehee, *Energy Environ. Sci.* **2014**, *7*, 3690.
[10] Z. Xiao, Y. Yuan, Y. Shao, Q. Wang, Q. Dong, C. Bi, P. Sharma, A. Gruverman, J. Huang, *Nat. Mater.* **2015**, *14*, 193.

[11] Y. Zhao, C. Liang, H. min Zhang, D. Li, D. Tian, G. Li, X. Jing, W. Zhang, W. Xiao, Q. Liu, F. Zhang, Z. He, *Energy Environ. Sci.* **2015**, *8*, 1256.

[12] Y. Zhang, M. Liu, G. E. Eperon, T. C. Leijtens, D. McMeekin, M. Saliba, W. Zhang, M. De Bastiani, A. Petrozza, L. M. Herz, M. B. Johnston, H. Lin, H. J. Snaith, *Mater. Horiz.* **2015**, *2*, 315.

[13] Y. Yuan, J. Chae, Y. Shao, Q. Wang, Z. Xiao, A. Centrone, J. Huang, *Adv. Energy Mater.* **2015**, 1500615.

[14] Z.-K. Tan, R. S. Moghaddam, M. L. Lai, P. Docampo, R. Higler, F. Deschler, M. Price, A. Sadhanala, L. M. Pazos, D. Credgington, F. Hanusch, T. Bein, H. J. Snaith, R. H. Friend, *Nat. Nanotechnol.* **2014**, *9*, 687.

[15] W. Tress, N. Marinova, T. Moehl, S. M. Zakeeruddin, M. K. Nazeeruddin, M. Grätzel, *Energy Environ. Sci.* **2015**, *8*, 995.

[16] a) K. Wojciechowski, S. D. Stranks, A. Abate, G. Sadoughi, A. Sadhanala, N. Kopidakis, G. Rumbles, C. Li, R. H. Friend, A. K.-Y. Jen, H. J. Snaith, *ACS Nano* **2014**, *8*, 12701. b) K. Wojciechowski, et al, *J. Phys. Chem. Lett.*, **2015**, 6 (12), 2399

[17] P.-W. Liang, C.-C. Chueh, S. T. Williams, A. K.-Y. Jen, *Adv. Energy Mater.* **2015**, 1402321.

[18] Y. Shao, Z. Xiao, C. Bi, Y. Yuan, J. Huang, *Nat. Commun.* **2014**, *5*, 5784.

[19] A. Walsh, D. O. Scanlon, S. Chen, X. G. Gong, S-H. Wei, arXiv:14117606v1 **2015**.

[20] C. Z. Li, C. C. Chueh, F. Ding, H. L. Yip, P. W. Liang, X. Li, A. K. Y. Jen, *Adv. Mater.* **2013**, *25*, 4425.

[21] D. Khim, K.-J. Baeg, M. Caironi, C. Liu, Y. Xu, D.-Y. Kim, Y.-Y. Noh, *Adv. Funct. Mater.* **2014**, DOI: 10.1002/adfm.201400850.

[22] a) J. T. W. Wang, J. M. Ball, E. M. Barea, A. Abate, J. a. Alexander-Webber, J. Huang, M. Saliba, I. Mora-Sero, J. Bisquert, H. J. Snaith, R. J. Nicholas, *Nano Lett.* **2014**, *14*, 724.

b) K. Wojciechowski, M. Saliba, T. Leijtens, A. Abate, H. J. Snaith, *Energy Environ. Sci.* **2014**, *7*, 1142.

[23] a) V. D'Innocenzo, A. R. S. Kandada, M. De Bastiani, M. Gandini, A. Petrozza, *J. Am. Chem. Soc.*, **2014**, 136 (51), 17730. b) M. De Bastiani, V. D'Innocenzo, S. D Stranks, H. J. Snaith, A. Petrozza, *Applied Physics Letters - Materials*, **2014,** 2 (8), 081509.

[24] C. Tao, S. Neutzner, L. Colella, S. Marras, A. R. S. Kandada, M. Gandini, M. De Bastiani, G. Pace, L. Manna, M. Caironi, C. Bertarelli, A. Petrozza, *Energy Environ. Sci.*DOI: 10.1039/c5ee01720c.

[25] J. S. Manser, & P. V. Kamat, *Nat. Photonics* **2014**, 8, 737.

[26] S. D. Stranks, G. E. Eperon, G. Grancini, C. Menelaou, M. J. P. Alcocer, T. Leijtens, L. M. Herz, A. Petrozza, and H. J. Snaith, Science, **2013**, 342, 341.

[27] (a) Yamada, Y.; Nakamura, T.; Endo, M.; Wakamiya, A.; Kanemitsu, Y. *J. Am. Chem. Soc.* **2014**, *136*, 11610; Stranks, S. D.; (b) Burlakov, V. M.; Leijtens, T.; Ball, J. M.; Goriely, A.; Snaith, H. J. *Phys. Rev. Appl.* **2014**, *2*, 034007. (C) Saba, M.; Cadelano, M.; Marongiu, D.; Chen, F.; Sarritzu, V.; Sestu, N.; Figus, C.; Aresti, M.; Piras, R.; Geddo Lehmann, A.; Cannas, C.; Musinu, A.; Quochi, F.; Mura, A.; Bongiovanni, G. *Nat. Commun.* **2014**, *5*, 5049.

[28] Y. Yuan, J. Chae, Y. Shao, Q. Wang, Z. Xiao, A. Centrone, J. Huang, *Adv. Energy Mater.* **2015,** DOI: 10.1002/aenm.201500615

[29] Donald Neaman, Semiconductor Physics and Devices,. 4th Edition, McGraw Hill Publications.

[30] C-Z. Li, C-Y Chang, Y. Z., H.-X. Ju, C.-C. Chueh, P-W Liang, N. Cho, D. S. Ginger, and A. K.-Y. Jen, *Adv. Mater.* **2014**, *26*, 6262–6267.

[ref aron] C. Eames, J. M. Frost, P. R.F. Bames, B. C. O'Regan, A. Walsh and M. S. Islam, *Nat. Comm.* **2015**, *6*, 7497.

[ref filippo] J. M. Azpiroz, E. Mosconi, J. Bisquert and F. De Angelis, *Energy Environ. Sci.* **2015**, *8*, 2118.

[ref del rev.] T-Y. Yang, G. Gregori, N. Pellet, M. Gratzel and J. Maier, *Angew. Chem.* **2015**, *127*, 8016-8021.

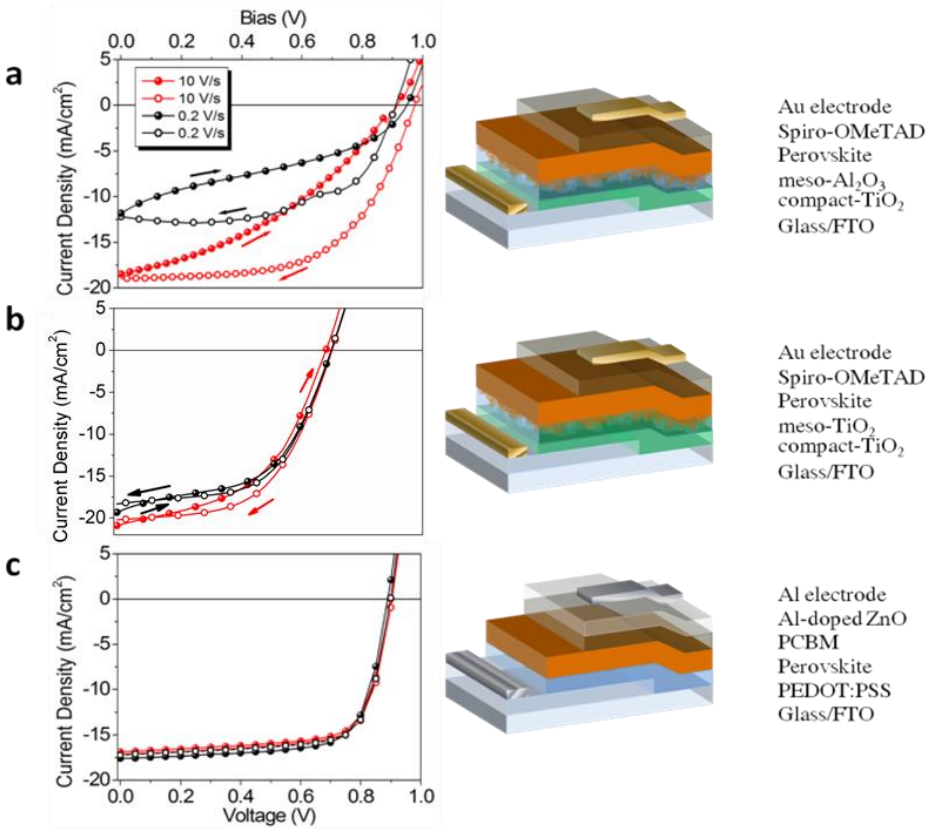

Figure 1. Current-voltage characteristics of three different device architectures measured under 1 sun. (a) Meso-alumina based device, (b) meso-TiO_2 based device, (c) inverted device. The current density is plotted as function of voltage scan direction (hollow dots: from open-circuit to short-circuit conditions, full dots: from short-circuit to open-circuit conditions) and as a function of the scan rate (red line 10 Vs^{-1}, black line 0.2 Vs^{-1}). For each device the sketch of the structure and the interlayers used are reported in the right panels.

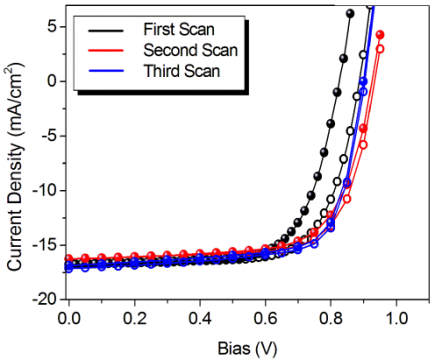

Figure 2. *J*/*V* characteristics of an inverted device (PEDOT:PSS/ $CH_3NH_3PbI_3$/PCBM) repeated several times consecutively. Hollow dots: from open-circuit to short-circuit conditions, full dots: from short-circuit to open-circuit conditions. Scan rate 10V/s. Scan starts at 1.4 V.

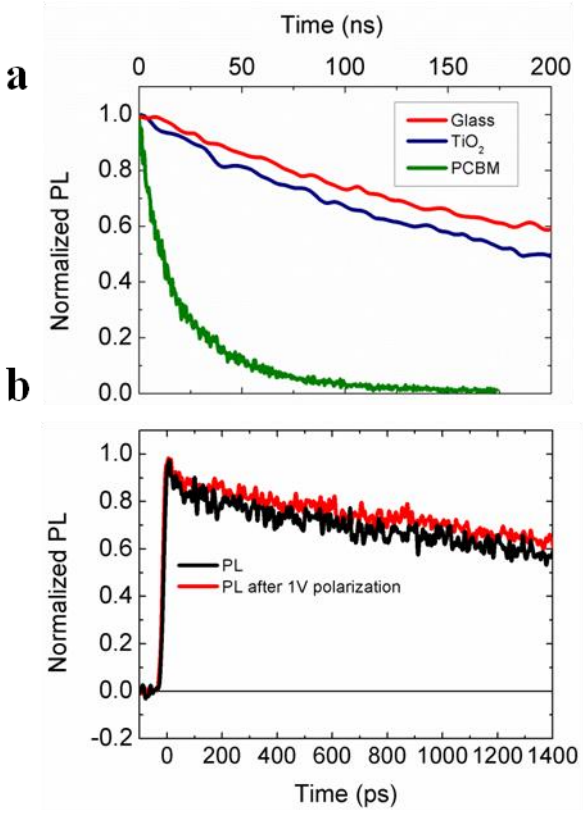

Figure 3. (a) PL dynamics from $CH_3NH_3PbI_3$ /TiO2 and $CH_3NH_3PbI_3$ /PCBM bilayer and from $CH_3NH_3PbI_3$ deposited on glass (probed wavelength 780nm, excitation wavelength 700nm); (b) PL dynamics from $CH_3NH_3PbI_3$ embodied in a solar cell architecture with PEDOT:PSS and PCBM as hole and electron extracting layer respectively. The device was under short-circuit condition before (black line) and after (red line) a pre-polarization (1V) treatment (probed wavelength 780nm, excitation wavelength 700nm).

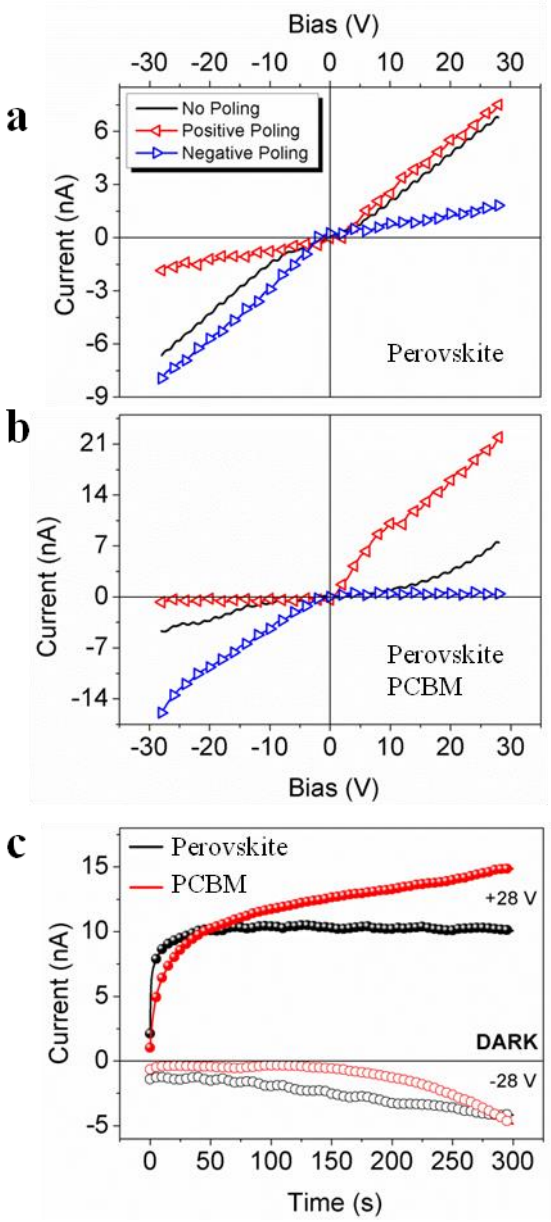

Figure 4. *I*/*V* curve of lateral symmetric devices under poling conditions of perovskite (a) and perovskite/PCBM (b): black line, no poling; red line, first polarization on a fresh sample; blue line, switched polarization on a fresh twin sample. The arrows indicate the directions of the

voltage scan. Scan rate = 25 Vs^{-1}, poling time = 120 s, field applied 1.4 $V\mu m^{-1}$. (c) Evolution of the dark current under poling condition for lateral devices of perovskite (black) and perovskite/ PCBM (red). These are fresh twin samples of those presented in (a) and (b). First polarization : full dots, switched: hollow circles. The inversion of the polarization is instantaneous. Voltage applied 1.4 $V\mu m^{-1}$

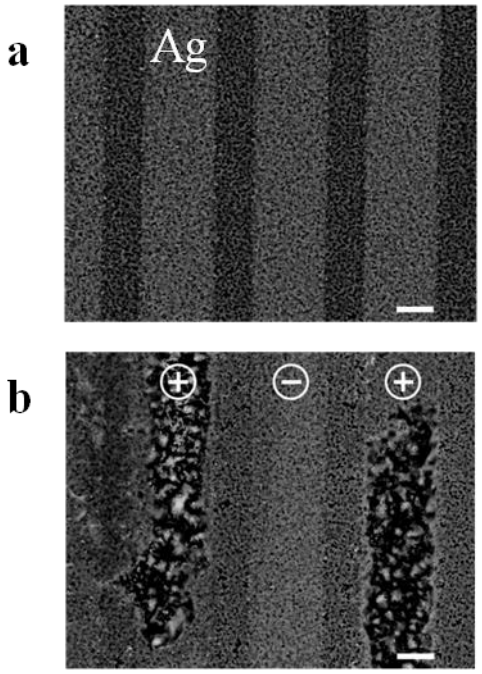

Figure 5. SEM top view of the perovskite lateral device with silver electrode before (a) and after the poling (b). The different electrode polarizations are reported with the "plus" and "minus" symbols. Scale bar 20 μm.

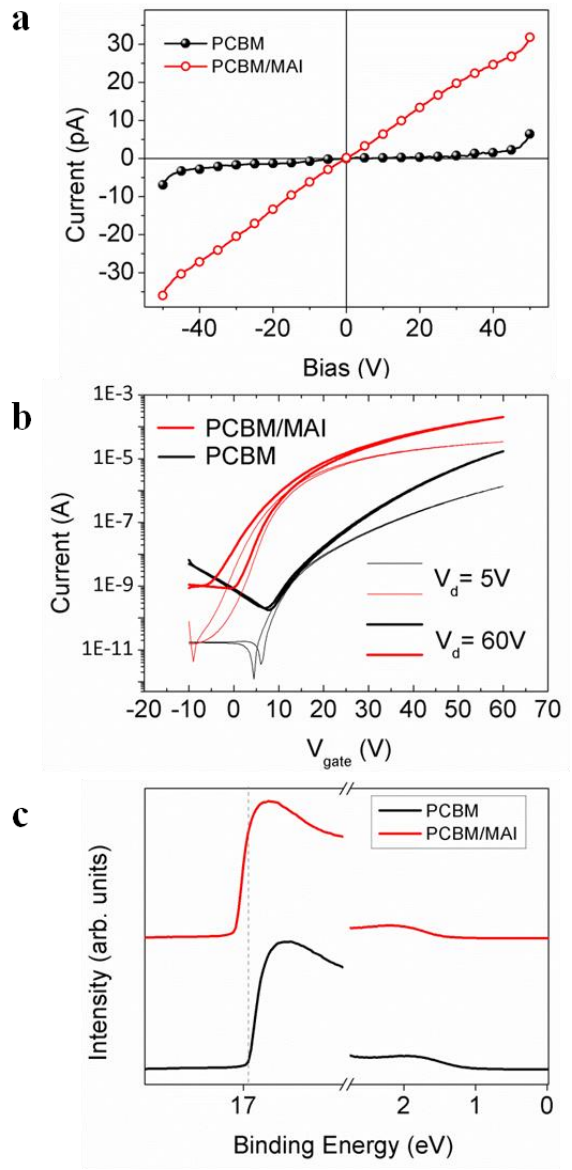

Figure 6. (a) J/V curves of a PCBM (black full dots) and PCBM/MAI (red open circles) films. (b) Transfer characteristics of the pristine PCBM top gate bottom contact transistor (black) and of the MAI doped PCBM device (red). Thick lines: saturation regime, thin line: linear regime. (c) UPS spectra showing the evolution of the Fermi level for a pristine PCBM (black) and PCBM:MAI (red) films.

Table 1. Performances of the standard and inverted perovskite solar cells vs. the voltage scan direction and the scan rate. OC: open-circuit, SC: short-circuit.

	Start Point [V]	End Point [V]	Stabilization Condition	Direction	Scan Rate [V/s]	Voc [V]	Jsc [mA/cm^2]	FF [%]	PCE [%]
TiO_2/Al_2O_3meso/ PVK/Spiro	1.4	0	Pre-Bias 1.4 V, 10 s Light	OC-SC	0.2	0.91	12.18	61	6.79
					10	0.97	18.97	58	10.76
	0	1.4		SC-OC	0.2	0.95	11.81	34	3.81
					10	0.92	18.46	37	6.31
TiO_2/TiO_2meso/ PVK/Spiro	1.4	0	Pre-Bias 1.4 V, 10 s Light	OC-SC	0.2	0.70	18.33	58	7.25
					10	0.70	20.22	55	7.78
	0	1.4		SC-OC	0.2	0.70	19.34	52	6.95
					10	0.68	20.9	49	6.90
PEDOT:PSS/ PVK/PCBM	1.4	0	Pre-Conditioning Cylces Light	OC-SC	0.2	0.90	17.22	72	11.23
					10	0.90	17.13	72	11.14
	0	1.4		SC-OC	0.2	0.90	17.59	72	11.25
					10	0.90	16.86	72	10.91

Table 2. Device parameter comparison for pristine PCBM and MAI doped PCBM transistors.

	Electron Mobility [cm^2/Vs]	Threshold Voltage [V]	I_{ON}/I_{OFF}	Subthreshold Slope [V/dec]
PCBM	$5.9\ 10^{-2}$	36.3	10^6	6
PCBM/MAI (30:1)	0.15	8.1	10^7	3

Supporting Information

Ions Migration and Role of the Electron Extracting Layer: Explaining the Need of Conditioning in Stabilized Hybrid Perovskite Solar Cells.

Michele De Bastiani, Giorgio Dell'Erba, Marina Gandini, Valerio D'Innocenzo, Stefanie Neutzner, Ajay Ram Srimath Kandada, Giulia Grancini, Maddalena Binda, Mirko Prato, Liberato Manna, James M. Ball, Mario Caironi and Annamaria Petrozza**

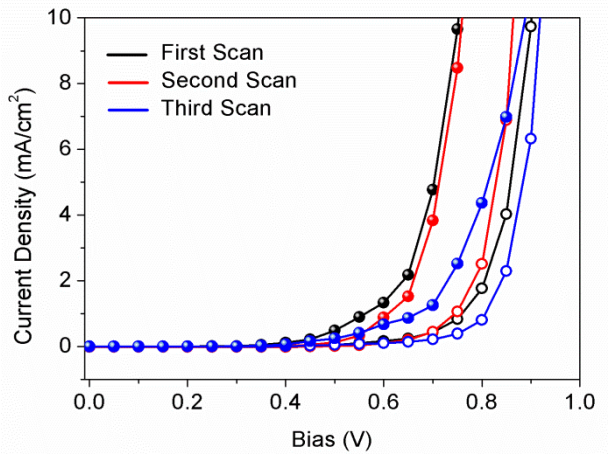

Figure S1. Consecutive scans of the dark *J*/*V* curve for an inverted PEDOT/perovskite/PCBM based device.

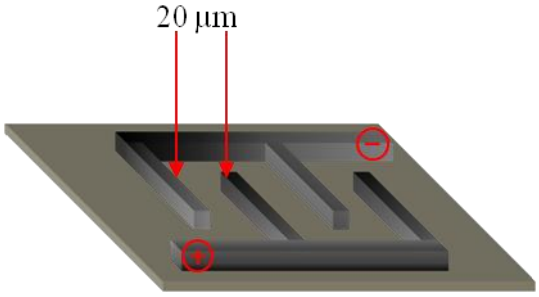

Figure S2. Sketch of the patterned electrodes used for the lateral devices. Electrodes can be both gold or silver. Thickness 15 nm.

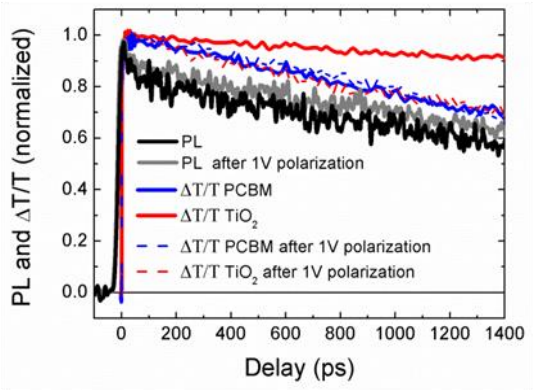

Figure S3.

PL dynamics from $CH_3NH_3PbI_3$ embodied in a solar cell architecture with PEDOT:PSS and PCBM as hole and electron extracting layer respectively. The device was under short-circuit condition before (gray line) and after (black line) a pre-polarization (1V) treatment (probed wavelength 780nm, excitation wavelength 700nm). The PL dynamics are compared to the Photo-bleach dynamics (dotted lines) measured by Transient absorption spectroscopy (ΔT/T) from $CH_3NH_3PbI_3$ (probed wavelength 760nm, excitation wavelength 650 nm) embodied in solar cell architectures with Spiro-Ometad as hole extracting layer and PCBM or TiO_2 as electron extracting layer.

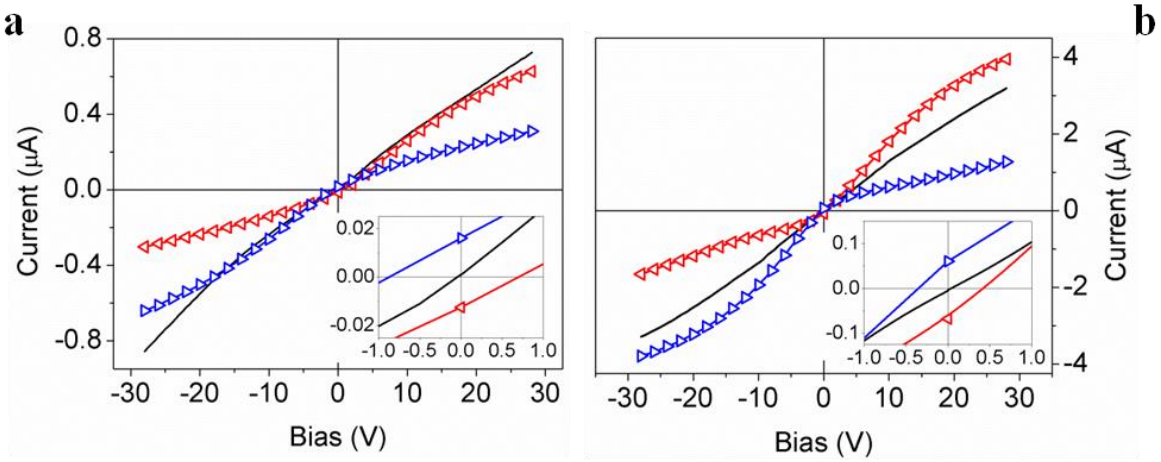

Figure S4. Effects of the poling under white light illumination (10 $mWcm^{-2}$) on a lateral device, with symmetric gold contacts, of perovskite and perovskite/PCBM. The length of the channel is 20 μm. Black line: no poling. Red line: positive poling. Blue line: negative poling.

The insets highlight biasing region around the short circuit condition where it is possible to detect the formation of a photocurrent and a photovoltage, according to the poling applied.

Carrier Concentrations. The electrons concentration is:

$$n = \frac{ni^2}{p} \quad (1)$$

With p the concentration of holes obtained by:

$$p = ni \ \ e^{\frac{Ef-Efi}{kT}} \quad (2)$$

With *Ef* the Fermi level of PCBM or PCBM:MAI from UPS measurements, *Efi* the intrinsic Fermi level considered at half of the PCBM bandgap, k the Boltzamann constant and T the absolute temperature. *ni* is the intrinsic carrier concentrations at thermal equilibrium:

$$ni = \sqrt{NcNv} \ \ e^{\frac{Eg}{2kT}} \quad (3)$$

With $Nc = 10^{21}$ cm^{-3} and $Nv = 10^{21}$ cm^{-3} density of state in the conduction and valence band respectively and *Eg* the energy gap of PCBM.

The table of contents entry should be 50−60 words long, and the first phrase should be bold. The entry should be written in the present tense and impersonal style.

Keyword: solar cells, hybrid perovskite, hysteresis, charge extracting layer, ions migration.

Michele De Bastiani, Giorgio Dell'Erba, Marina Gandini, Valerio D'Innocenzo, Stefanie Neutzner, Ajay Ram Srimath Kandada, Giulia Grancini, Maddalena Binda, Mirko Prato, James M. Ball, Mario Caironi and Annamaria Petrozza**

Ions Migration and Role of the Electron Extracting Layer: Explaining the Need of Conditioning in Stabilized Hybrid Perovskite Solar Cells.

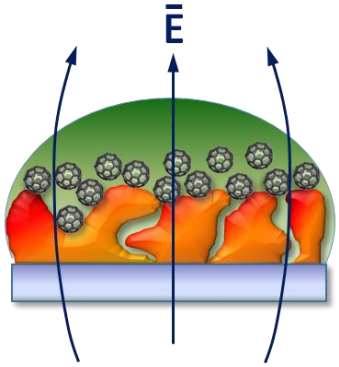

626
627